Estimation of Aerosol Single Scattering Albedo from Solar Direct Spectral Radiance and Total Broadband Irradiances

Fengsheng Zhao[1,2], Zhanqing Li[1]

1. ESSIC and Dept of Atmospheric & Oceanic Science
University of Maryland, College Park, MD 20740
2. National Satellite Meteorological Center, Beijing 100081, China

Submitted to

Special Issue on East Asian Study of Tropospheric Aerosols: an International Regional Experiment (EAST-AIRE)

Journal of Geophysical Research

April 7, 2006

Abstract

Aerosol single scattering albedo (ω_o) is a primary factor dictating aerosol radiative effect. This study presents a method of retrieving ω_o using spectral direct radiance measurements or aerosol optical depths together with total sky irradiance. The method does not require sky radiance data that can only be acquired by the expensive scanning sun-photometer. The method is evaluated using extensive measurements made by a suite of instruments deployed in northern China under the East Asian Study of Tropospheric Aerosols, an International Regional Experiment (EAST-AIRE) project. The sensivities of the retrieval to various uncertain factors were first examined by means of radiative transfer simulations. It was found the retrieval is most sensitive to cloud screening, total irradiance and the Angstrom Exponent (AE), but only weakly depends on surface albedo and the fine structure of aerosol size distribution. Using one-year of rigorously screened clear-sky measurements made at the Xianghe site, the retrieved ω_o values agree with those retrieved from the Cimel sun-photometer by the AERONET method to within ~0.03 (RMS), and ~0.003 (mean bias). As part of the differences originate from different sky views seen by the sun-photometers and pyranometer under comparison, a further test was conducted by using total sky irradiances simulated with the retrieved aerosol properties from the AERONET. The resulting estimates of ω_o agree to within 0.01-0.02 (RMS differences) and 0.002-0.003 (mean bias). These values are better measure of the true retrieval uncertainties, as they are free from any data mismatch. The characteristics of ω_o retrievals were discussed. It is worthy noting that the method requires reliable cloud screening.

1. Introduction

Aerosols have a significant impact on global climate, either directly through scattering and absorption of solar radiation [*Coakley et al.*, 1983; *Charlson et al.*, 1992; *Kiehl and Briegleb*, 1993; *Boucher and Anderson*, 1995; *Schwartz*, 1996] or indirectly by modifying the microphysical properties of clouds [*Twomey*, 1977; *Twomey et al.*, 1984; *Coakley et al.*, 1987; *Albrecht*, 1989]. Aerosol absorption of solar radiation may also affect cloud formation and cloud amount [*Hansen et al.*, 1997; *Ackerman et al.*, 2000].

In recent decades, increasing effort has been devoted to the estimation of aerosol climate effects. Direct radiative forcing is estimated to be -0.4 Wm^{-2} for sulphate aerosols, -0.2 Wm^{-2} for biomass-burning aerosols, -0.1 Wm^{-2} for fossil fuel organic carbon, and $+0.2$ Wm^{-2} for fossil fuel black carbon aerosols [*Intergovernmental Panel on Climate Change*, 2001]. These estimates are subject to very large uncertainties. A chief cause for the large uncertainties is the lack of reliable information on the spatial and temporal distribution of aerosol properties. The aerosol single scattering albedo, ω_o, defined as the fraction of the aerosol light scattering over the total extinction, is one of the most important properties of aerosols. The direct radiative effect of aerosols is very sensitive to ω_o. For example, a change in ω_o from 0.9 to 0.8 can alter the sign of the direct effect, depending on the albedo of the underlying surface, aerosol backscattering fraction etc. [*Chylek and Coakley*, 1974; *Hansen et al.*, 1997].

Due to technical difficulties, few instruments can measure this key aerosol variable directly. To date, the most widely used means of obtaining aerosol ω_o on large scales and on a routine

basis is to retrieve it using ground-based sunphotometer data from the Aerosol Robotic Network (AERONET) (http://aeronet.gsfc.nasa.gov/) [*Holben et al.*, 1998]. The AERONET network has been successfully developed for long-term observations at over 349 stations worldwide and includes measurements of direct spectral solar and sky radiation using sunphotometers. Observations of the direct irradiance and the angular distribution of sky radiances at 0.44, 0.67, 0.87, and 1.02 μm are used to derive aerosol optical depth, size distribution and ω_o [*Dubovik et al.*, 2000, 2002]. Accurate retrievals of ω_o (with accuracies reaching 0.03) can be obtained for high aerosol loadings and for solar zenith angles $>50^0$.

A pioneering study in retrieving aerosol properties from ground-based observations was conducted by *King and Herman* [1979] and *King* [1979] where a statistical algorithm was proposed for inferring the imaginary part of the aerosol index of refraction and surface albedo from the diffuse and direct solar radiation measurements. The algorithm works reasonably well in the case of a clear atmosphere devoid of any cloud cover for a long enough period of time with a large range of change in the solar zenith angle ($\sim 40^o$). A combination of measurements from a sunphotometer, a sky radiometer and a total broadband radiometer were also employed to derive broadband aerosol ω_o by *Silva et al.* [2002]. More recently, *Kassianov et al.* [2005] described a technique to retrieve aerosol column number density, mean radius and ω_o from observations made by the multifilter rotating shadowband radiometer. Compared to the measurements from AERONET, this technique has a higher temporal resolution (~ 20 s) and its accuracy is independent of the solar zenith angle. The technique can be successfully applied to cases where the aerosols are mainly composed of fine mode particles. If the relative contribution

of coarse or giant particles (1 μm and larger) is significant, their technique fails to retrieve the aerosol properties.

In this study, aerosol ω_o is retrieved using measurements of spectral direct solar radiation and broadband downwelling total solar radiation acquired in China for an entire year from 2004 to 2005. In our retrieval algorithm, sky radiation measurements are not needed. The retrieval accuracy is shown to be compatible with those from the AERONET retrievals for cases where both coarse and fine particles are abundant. Also, the accuracy does not deteriorate badly for small solar zenith angles. The proposed method has significant potential implications for studying aerosol effects on regional climate. Aerosol absorption in China has drawn much attention in recent years [e.g., *Menon et al.*, 2002]. However, little quantitative information is available. Under the auspices of the East Asian Study of Tropospheric Aerosols: an International Regional Experiment (EAST-AIRE) project [*Li et al.*, 2006], a network of 25 stations spread throughout China provides measurements of direct spectral solar radiation [*Xin et al.*, 2006] that may be used, in combination with total irradiance measurements, to provide nationwide estimates of aerosol ω_o.

In section 2, sensitivity analyses of ω_o to broadband fluxes, size distribution and ground surface albedo are presented. In section 3, the proposed algorithm to retrieve aerosol ω_o is discussed. Section 4 describes the observation site from which measurements used in this study were made, the instrumentation deployed and data processing procedures. Application of the algorithm and analysis of the ω_o retrievals are given in section 5. A comparison with the AERONET retrievals is presented in section 6. Detailed error analyses are performed in section 7

and a summary of the results and conclusions is given in section 8.

2. Sensitivity Analyses

To gain insight into the dependence of the surface broadband downwelling shortwave (SW) fluxes on aerosol properties and ground surface albedo, sensitivity analyses were performed using a modified radiative transfer code developed by *Nakajima and Tanak*a [1988] that includes the K-distribution method [*Kneizys et al.*, 1988] for gas absorption; molecular scattering is also included. The gas vertical profile is given by the U.S. standard atmosphere [*McClatchey et al.*,1972]. The real part of the aerosol index of refraction is fixed and equal to 1.5. The aerosol ω_o varies with changes in the imaginary part of the index of refraction and the size distribution of aerosols. The aerosol size distributions used in the calculations are the Junge power law distribution and the bimodal distribution. The Junge power law is expressed as:

$$dv(r)/d\ln r = \begin{cases} c(r/0.1)^4 & r \le 0.1\mu m \\ c(r/0.1)^{-(p-4)} & r > 0.1\mu m \end{cases} \quad (1)$$

where dv(r)/dlnr is the aerosol volume spectrum at particle radius r, c is a constant, and p is the exponent of the Junge power law. The bimodal distribution is expressed as:

$$dv(r)/d\ln r = c_1 \times \exp\left(-\left(\ln r - \ln r_{01}\right)^2 / 2\ln\sigma_1\right) + c_2 \times \exp\left(-\left(\ln r - \ln r_{02}\right)^2 / 2\ln\sigma_2\right) \quad (2)$$

where the subscripts 1 and 2 correspond to fine and coarse particle modes, respectively, r_{01} and r_{02} are their mode radii, σ_1 and σ_2 are their geometric standard deviations, c_1 and c_2 represent the peak values of the two modes and the ratio c_2/c_1 is the peak ratio which indicates the dominance

of the two modes. The particle size radius in the calculations ranges from 0.01 μm to 15 μm.

Figure 1a shows the surface broadband downwelling SW fluxes calculated with different values of ω_o derived from the Junge power law distribution with an exponent fixed at 4.2. The abscissa in Figure 1 is the aerosol optical depth at 0.5 μm. The fluxes are sensitive to ω_o and this sensitivity increases with increasing aerosol optical depth. With increasing aerosol optical depth, the photon pathlength increases and the probability of absorption increases. This implies that the accuracy of the retrieval of ω_o from broadband solar fluxes increases with the aerosol loading. The tendency of increasing retrieval errors with a decrease in the aerosol optical depth was also found in the detailed accuracy assessments of aerosol optical properties retrieved from AERONET [*Dubovik et al.*, 2000]. They concluded that for sun and sky radiance measurements, accurate retrievals can only be obtained under high aerosol loading conditions.

Figure 1b shows the surface broadband downwelling SW fluxes calculated using different exponents in the Junge power law expression. The broadband fluxes increase rather dramatically with increases in the magnitude of the exponent. It is well known that the Angstrom exponent, α, is related to the Junge power law exponent through the relation

$$\alpha = p - 3. \qquad (3)$$

The value α describes a regression relationship between aerosol optical depths and wavelengths according to the expression

$$\tau(\lambda) = \beta\lambda^{-\alpha} \qquad (4)$$

where τ is the aerosol optical depth at wavelength λ and β is a constant. It follows from equations 3 and 4 that the larger the value of p, the faster the optical depth decreases with

increasing λ. So for the same value of optical thickness at 0.5 μm, the larger the value of p and the larger the surface broadband downwelling SW flux. Estimation of ω_o from surface broadband downwelling SW fluxes thus requires information on the aerosol size *a priori* or simultaneously.

Although the Junge power law distribution has been widely used, many observational studies in recent decades show that the fine structure of the aerosol size distribution may be best described by the bimodal distribution of equation 2. It is of interest to look at the difference between the broadband downwelling SW fluxes calculated using the Junge power law distribution and the bimodal distribution for the same value of α.. Figure 1c shows the broadband downwelling SW fluxes calculated using the bimodal distribution with the following parameters: $r_{01} = 0.15$ μm; $r_{02} = 4$ μm; $\sigma_1 = 2.5$; $\sigma_2 = 4.5$, and $c_1/c_2 = 1$. We first calculated the spectral optical depth using the bimodal distribution then a linear regression technique is used to obtain α. The exponent p of the Junge power law distribution is calculated from equation 3 using this α.. It appears that the detailed structure of the size distribution has little effect on the broadband downwelling SW fluxes, indicating that the Junge power law can be used to approximate the bimodal distribution, provided that the Angstrom exponents derived from the two distributions are the same. This was also noted in *Zhao et al.* [1997, 2002], where they illustrated the validity of using the Junge power law in the satellite remote sensing of aerosols.

Figure 1d shows the broadband downwelling SW fluxes calculated using different values for ground surface albedo. The magnitudes of the ground surface albedo are divided into two groups: one with magnitudes around 0.15 and the other with magnitudes around 0.75. The magnitudes of the broadband downwelling SW fluxes increases with increasing surface albedo due to

multiple reflections. The surface albedo can be derived from satellite observations of broadband and narrowband radiances (such as MODIS, AVHRR, ERBE, CERES, etc.) with an accuracy of about 0.01~0.03 [e.g., *Li and Garand*, 1994; *Li et al*., 2002; *Liang*, 2003; *Liang et al.*, 2005].Uncertainties in the surface albedo result in negligible errors in the broadband downwelling SW fluxes, e.g. an uncertainty of 0.05 in the surface albedo results in an error of less than about 4 Wm^{-2} in the broadband downwelling SW fluxes.

3. Algorithm for determination of ω_o

According to the sensitivity analyses described above, for a fixed aerosol optical depth, the broadband downwelling SW fluxes depend mainly on ω_o and the spectral optical depth from which the Angstrom exponent, or the Junge power law exponent, can be calculated. An algorithm is developed to determine the aerosol ω_o from the observations of broadband downwelling SW fluxes and aerosol spectral optical depths. The imaginary part of the index of refraction is first estimated by matching measured and calculated broadband downwelling SW fluxes. In the flux calculations, the aerosol optical thickness at 0.5 μm and α is used. The aerosol size distribution is approximated by the Junge power law with its exponent calculated from the Angstrom exponent. An assumption is that the imaginary part of the index of refraction is independent of wavelength in the SW spectral region. We have performed numerical experiments to investigate the validity of the assumption. The results show that the assumption may cause errors of 0.03-0.04 in the case of hematite mixed with other mineral particles. However, for most aerosol types, such as

rural, urban and dust-like aerosols, the results of the numerical experiments indicate that the wavelength independence assumption is reasonable. Especially, for the urban aerosol models in which black carbon absorption is dominating, the retrieved errors are less 0.01. The effect of water vapor on the broadband downwelling SW fluxes is considered in the flux calculations. The column precipitable water amount is obtained from either satellite remote sensing [e.g., *Gao and Goetz*, 1990; *Kaufman and Gao*, 1992; *Bartsch and Fischer*, 1997; *Gao and Kaufman*, 2003] or sunphotometer measurements [e.g., *Volz*, 1974; *Bird and Hulstrom*, 1982; *Halthore et al.*, 1997; *Morys et al.*, 2001]. Surface reflection is assumed to be Lambertian. The broadband downwelling SW fluxes are calculated using different values of the imaginary part of the index of refraction until the absolute differences between calculated and measured broadband downwelling SW fluxes are less than 1 Wm^{-2}. The spectral aerosol ω_o is then calculated from the index of refraction and the Junge power law size distribution.

4 Observation site, instrumentation and data processing

This study was conducted under the auspices of the EAST-AIRE project whose goal is to gain basic knowledge about the characteristics of aerosols and gases in China and an understanding of their climatic effects in China [*Li et al.*, 2006]. To this end, extensive facilities have been (and will continue to be) established including both supersites and a nationwide observational network [*Xin et al. 2006*]. Field campaigns conducted on the ground and from the air were carried out in the spring of 2005 and plans for future campaigns are underway. The first super-station set up in

Xianghe (39.75^{0}N, 116.38^{0}E) is located 70 km east of Beijing and has a population of 310 000. The site has provided extensive measurements since the fall of 2004, including 1) radiative quantities (direct, diffuse and total SW and longwave fluxes) using broadband and narrowband radiometers, and spectrometers; 3) aerosol optical quantities (optical depth, scattering and absorbing coefficients, vertical attenuation profiles) using a Cimel sunphotometer, nephelometer, aethalometers, PSAP, etc.; 3) cloud properties (whole sky cloud views, optical depth, cloud height, liquid water path); 4) aerosol quantities (optical depth, ω_0, size distribution, mass and condensation number); 5) aerosol composition; and 6) precursor gases amounts (ozone, NO, NOx, NOy, CO, SO2).

This study employs a small subset of observations made at Xianghe. The site is under the influence of the East Asian monsoon. From October to April, northwestly winds prevail, blowing in air from Siberia and the Mongolia Plateau. During the spring season, the strong winds may transport desert dust and pollutants from Beijing to Xianghe, affecting local aerosol properties [*Eck et al.*, 2005]. During the summer season, southeastly winds are dominant and aerosol properties may be affected by humid oceanic air. The sulfate and carbonaceous particles produced by fossil fuel combustion and biomass burning are important components of the local aerosols. Except for summer, the climate in other seasons is dry. Locally produced windblown dust particles are also an important component of aerosols.

Primary data used in this study are spectral solar direct radiation and broadband downwelling SW fluxes measured by a CIMEL CE-318 sunphotometer and a Kipp & Zonen CM21 pyranometer, although data from several other instruments were employed for selecting

cloud-free measurements and for data quality control (described later). The sunphotometer measures the direct solar radiation at 0.340, 0.380, 0.440, 0.500, 0.675, 0.870, 0.940, and 1.020 μm with a 1.28^{o} full field of view. Details of instrument calibration and data processing are described in *Holben et al.* [1998]. The errors in the derived aerosol optical depth are less than 0.01 for wavelengths >0.44 μm and 0.02 for shorter wavelengths. The Kipp & Zonen CM21 pyranometer is used to measure the broadband downwelling SW fluxes in the 0.305-2.80 μm spectral range. The instrument response time is 5 seconds and the data sampling time interval is 1 minute. The measurement error of the instrument is estimated to be less than 10 Wm^{-2}. As a quality control measure, total irradiance was also observed simultaneously with three other instruments, namely a Kipp & Zonen Cimel-11, and Eppley 8-48 black and white pyranometer and normal incidence pyrheliometer. The Eppley instruments were mounted on a solar tracker to measure the direct and diffuse radiation. Discrepancies in total irradiance measurements made by the three independent instruments are usually within 5 Wm^{-2} and rarely exceed more than 10 Wm^{-2}. Larger discrepancies occurred occasionally for which the causes were identified and the data were promptly corrected using independent measurements. The data have been collected continuously from September 2004 till the present.

A critical step of the data processing for this study is separation of cloud-affected data from cloud-free data because the retrieval of aerosol ω_o is susceptible to cloud contamination. A cloud-screening method proposed by *Smirnov et al.* [2000] was applied to AERONET data so that clear-sky data were selected in order to retrieve the aerosol optical depths. However, this method only identifies a cloud-free path between the sunphotometer and the solar disk, while the

retrieval proposed by this study requires a hemispheric cloud-free sky. A much more rigid cloud screening method was performed that employed time series of radiation data and total sky images of high frequency obtained from a Total Sky Imager (TSI-440A) manufactured by Yankee Environmental Systems [*Li et al.*, 2006]. Only sunphotometer measurements made when the whole sky is clear are employed in this study for two reasons. First, the aerosol optical depths are used together with surface total irradiance to retrieve the aerosol ω_o. One may question the necessity for doing this, given that ω_o can be retrieved from sunphotometer measurements. It should be borne in mind that retrieving ω_o requires sky radiance data that can only obtained by using a complicated and thus expensive Cimel sunphotometers. However, observing the aerosol optical depth can be achieved with a much simpler and cheaper device such as the hand-held sunphotometers. The second usage of the subset of Cimel data is to evaluate the retrieval of ω_o by comparing the two types of retrievals.

5 Results and discussion

The algorithm described in section 3 was applied to retrieve ω_o by combining aerosol optical depths at 0.5 μm, Angstrom exponents ($\alpha_{440\text{-}870}$), precipitable water amounts and observed broadband downwelling SW irradiances. According to the sensitivity analyses described in section 2, the retrieval of ω_o is only feasible for moderate and high aerosol loading. Only data with aerosol optical depths larger than 0.4 (at 0.44 μm) were selected for the analyses. The same constraint was applied in the AERONET retrievals of aerosol optical properties [*Dubovik et al.*,

2002]. Such heavy aerosol loading is often observed at the Xianghe site [*Li et al., 2006b*].

Data from September 2004 to August 2005 were analyzed with a total of 8513 samples. Figure 2 shows the statistics for the retrieved values of ω_o. The average value is 0.9, with 50.4% of the retrieved values larger than 0.9, 48.3% between 0.80-0.9, and 1.3% smaller than 0.8. The average value of ω_o is nearly the same as those reported for Mexico City and the Maldives [*Dubovik et al.*, 2002]. Aerosols with such values for ω_o can have a cooling or warming effect on the climate over land surfaces, pending on the magnitude of the surface albedo. The broadband surface albedo around the Xianghe site is about 15%, resulting in a neutral aerosol effect. Matching irradiance data at the top of the atmosphere (TOA) obtained by the Clouds and the Earth's Radiant Energy System instrument with ground-based aerosol data, *Li et al. [2006]* found that aerosols do not alter the radiation budget at the TOA regardless of aerosol loading, although they substantially reduce the surface radiation budget. This implies that there is strong atmospheric heating due to the aerosols. For the cases with $\omega_o < 0.8$, these aerosols contain black carbon particles which are a highly absorbing species resulting from either industrial combustion or incomplete biomass combustion. Such aerosols have a heating effect on the climate in general.

The magnitude of the Angstrom exponent is determined by the fraction ratio of fine and coarse modes. If the coarse mode is predominant, the Angstrom exponent is small, and vice-versa [*Eck et al.*, 2005]. Figure 3a shows the scatterplot of ω_o as a function of the Angstrom exponent. Although the data shown in the figure are rather dispersed, a general trend can be seen: ω_o tends to decrease with increasing Angstrom exponent (increase in the fraction of fine-model particles). Fine-mode particles primarily originate from fossil fuel combustion and biomass

burning, as well as by the oxidation of gaseous compounds such as sulfur dioxide, nitrogen oxides, and volatile organic compounds. Among these constituents, the black carbon particles from incomplete fossil fuel combustion and biomass burning are the strongest light absorbers. Therefore, an increase in the concentration of fine mode particles tends to reduce ω_o. In the Xianghe area under high aerosol loading, the coarse mode particles mainly consist of mineral dust. An increase in the dust particle concentration tends to increase the ω_o of the polydispersion. In previous studies, the values of ω_o reported from model simulations [e.g. *Shettle and Fenn*, 1979; *WMO,* 1983; *Koepke et al.*, 1997; *Hess et al.*, 1980], in situ measurements [e.g., *Patterson et al.*, 1977; *Haywood et al.*, 2001] and column-averaged retrievals [*Kaufman et al.*, 2001; *Tanre´ et al.,* 2001; *Dubovik et al.*, 2002] vary considerably, rendering a necessity to measure in different parts of the world.

Figure 3b shows that ω_o increases with increasing aerosol optical depth, indicating that for higher aerosol loading, fossil fuel combustion and biomass burning are not the predominant factors causing the increase in the concentration of aerosols. Heavy aerosol episodes appear to be caused, more likely, by blowing mineral dust. This is partially confirmed by the relationship between aerosol optical depth and the Angstrom exponent as shown in Figure 3c.

Figure 4a shows the daily-averaged values of ω_o at λ=0.5μm. The dramatic day-to-day variation shown in this figure may be related to meteorological conditions, including variations in air parcel trajectory, humidity, temperature inversions, and dust particles driven by high winds. The seasonal variation shown in Figure 4b indicates that ω_o has a minimum in spring and a maximum in summer. As described before, in the spring season, northwesterly winds prevail,

driving the air pollution from Beijing to the Xianghe site (downwind). *Eck et al*. [2005] studied the spatial relationship of aerosol properties. They illustrated that in spring, aerosol properties between Beijing and Xianghe are highly correlated, suggesting that the aerosol properties observed in Xianghe are significantly affected by the pollutants from Beijing during this season. The summer maximum in the magnitude of ω_o indicates that the emission of black carbon during this season is minimum, consistent with the trend in the seasonal variation of black carbon emission in China [*Streets et al.*, 2003]. In addition, the relatively humid air from the southeast and rainy weather (about three quarters of the annual precipitation at Xianghe occurs during the summer season) may be another important factor for the summer minimum in the magnitude of ω_o.

6. Comparison with AERONET retrievals

To assess the validity of our retrievals, the values of ω_o retrieved by our algorithm are compared with those from AERONET. The two retrievals occur on different time scales: 1 minute for the retrievals from the proposed algorithm and about 1 hour for the AERONET ω_o. To match the times for comparison purposes, the values of ω_o from the proposed algorithm were averaged over a period of 30 minutes before and after the times corresponding to the AERONET retrievals. Figure 5a-d shows comparisons of ω_o at 0.44 μm, 0.67 μm, 0.87 μm and 1.02 μm, respectively. Both products are limited to optical depths larger than 0.4 at 0.44 μm and solar zenith angles larger than 50^0. The standard deviations and mean differences are 0.0218, 0.024,

0.03, 0.0369 and 0.0028, 0.0028, 0.0054, 0.0108 at 0.44, 0.67, 0.87 and 1.02 μm, respectively. Since the contribution of the scattered radiation at 0.44 and 0.67 μm to the SW flux is much larger than that at 0.87 and 1.02 μm, the accuracies of the retrievals are higher at visible wavelengths than in the near infrared. The same is true for the AERONET retrievals [*Dubovik et al.*, 2000]. It is thus not surprising that the difference between the two retrievals is smaller in the visible than in the infrared. Considering that the accuracy of the AERONET ω_o retrievals is on the order of 0.03, the consistency between our retrievals and AERONET products is satisfactory.

7. Error Analyses

Despite the good agreement shown in Figure 5, attempts are made to gain further insights into the discrepancies in terms of input data uncertainties and assumptions made in the retrieval algorithm.

7.1 Effects of instrument measurement errors

The instruments used in the present study are the CIMEL CE-318 sunphotometer and the Kipp & Zonen CM21 pyranometer. The CIMEL CE-318 sunphotometer is well calibrated by the AERONET group at least once a year. The errors in the aerosol optical depth derived by this instrument are less than 0.01~0.02. Such errors can induce negligible uncertainties in the calculation of broadband downwelling SW fluxes. For example, for a solar zenith angle of 50^0, an error of 0.01 in the aerosol optical depth at 0.5 μm can cause an error of 1.7 Wm^{-2} in the SW fluxes, assuming an Angstrom exponent equal to 1.2.

The effects of the CM21 pyranometer measurement errors on the retrieved ω_o are shown in Table 1. In this table, the instrument measurement error is fixed at 8 Wm^{-2} (the errors of CM21 measurements are estimated to be less than 10 Wm^{-2}). As previously mentioned, the errors in the retrieved ω_o increase with decreasing aerosol optical depth. For aerosol optical depths > 0.4, the retrieval errors are less than 0.03. Such errors are comparable to those retrieved from the observations of sun/sky radiation under high aerosol loading conditions [*Dubovik et al.*, 2002].

7.2 Errors due to assumptions

In the present algorithm, the Junge power law is used to describe the aerosol size distribution in an actual atmosphere. It is also assumed that the real part of the index of refraction of aerosols is independent of wavelength and has a fixed value of 1.5. To investigate the uncertainties incurred by invoking these assumptions, many experiments were conducted. First, surface broadband downwelling SW fluxes were simulated using the AERONET retrievals of aerosol size distribution and index of refraction at the Xianghe site. The simulated broadband downwelling SW fluxes, in conjunction with the AERONET aerosol optical depth and Angstrom exponent products, were then employed to retrieve ω_o using the proposed algorithm. Figure 6 presents the comparison of ω_o retrieved from our algorithm using the simulated surface total irradiances with those retrieved by the AERONET using sky radiances. In this case, the AERONET products are considered as 'true' values. The standard deviations and mean errors are 0.013, 0.013, 0.016, 0.022 and 0.0024, 0.0032, 0.0042, 0.0102 at 0.44, 0.67, 0.87 and 1.02 μm, respectively. Such errors are not significant, especially for the visible spectral region. *Dubovik et*

al. [2000] found that under error-free conditions, the retrieval accuracy due to computation errors can reach 0.01.

The agreement shown in Figure 6 is a better indication of the true retrieval accuracy of the retrieval algorithm because of the different fields of view seen by the sunphotometer and the pyranometer. Note that the AERONET retrievals of aerosol properties are based on direct solar radiance and sky radiance measurements over a small portion of the sky, while our retrieval is sensitive to both direct radiation and diffuse radiation from the entire sky dome. Any discrepancy would transform into a retrieval disagreement. For example, if a portion of the sky outside the sunphotometer viewing domain is covered by an undetected residual cloud, the two retrievals would differ considerably, simply because they did not see the same targets. Likewise, inhomogeneous aerosol distribution in the sky also incurs a disagreement. As such, the retrievals shown Figure 6 represent the true uncertainties induced by the retrieval algorithm *per se*, as the differences caused by a major input variable, namely, the surface irradiance, is removed.

Another retrieval error suffered by most aerosol retrieval algorithms is incurred by the assumption that the aerosol particles are spherical. The validity of such an assumption was discussed by many investigators [e.g., *Koepke and Hess*,1988; *Mishchenko et al.*,1995, 1997]. *Mishchenko et al.* [1997]. It was found that differences in the scattering phase functions between spherical and non-spherical particles can be large, but differences in the optical cross-sections, ω_o and asymmetry parameter are much smaller (less than a few percent under most circumstances). Use of broadband irradiances instead of radiance in our algorithm lowers the sensitivity of the retrieval to particle shape. Therefore, the spherical particle assumption may not

induce significant errors in the ω_o retrieved by the proposed algorithm.

8. Summary and Conclusions

In this study, we attempt to estimate the aerosol ω_o from combined measurements of spectral direct solar radiation and broadband downwelling SW fluxes. Tests were performed to examine the sensitivity of the broadband fluxes to aerosol ω_o, size distribution and the ground surface albedo. An algorithm was developed according to the sensitivity analyses. In our algorithm, we first determine the imaginary part of the index of refraction by comparing the measured broadband downwelling SW fluxes with those calculated using the optical thickness at 0.5 μm and the Angstrom exponent. The aerosol size distribution follows the Junge power law and the real part of the index of refraction is fixed at 1.5. The aerosol ω_o is calculated by using the retrieved index of refraction and the Junge power law size distribution.

The algorithm was applied to measurements made in Xianghe, China from September 2004 to August 2005 under the auspices of the EAST-AIRE project. The cloud screening was carefully performed by using the movie of the sky conditions obtained from the Total Sky Imager (TSI-440A). The average value of the retrieved ω_o at 0.5μm is 0.9, with 50.4% of the retrieved values larger than 0.9, 48.3% between 0.80-0.9, and 1.3% smaller than 0.8. It varies considerably from day to day. In general, the seasonal variation of ω_o is much less pronounced than the day-to-day variation with a minimum in the spring and a maximum in the summer. The ω_o decreases as the Angstrom exponent increases, implying that the finer aerosol particles have stronger absorption than the

coarser aerosol particles. This indicates that emissions from fossil fuel combustion and biomass burning are major contributors to the aerosol absorption. The majority of the heavy aerosol episodes have large ω_o, presumably due to an increasing proportion of mineral dust.

The values of ω_o retrieved from our method are compared with the AERONET product. The two retrievals agree fairly well with each other. The standard deviations and mean differences are 0.0218, 0.024, 0.03, 0.0369 and 0.0028, 0.0028, 0.0054, 0.0108 at 0.44, 0.67, 0.87 and 1.02 μm, respectively. A significant fraction of the discrepancies originate from differences in the fields of view of the pyranometer and sunphotometer, as indicated by the differences in surface irradiances measured by the pyranometer and those computed from the AERONET-based retrievals of aerosol parameters. If the same surface irradiances were used, the standard deviations and mean errors would be lowered to 0.013, 0.013, 0.016, 0.022 and 0.0024, 0.0032, 0.0042, 0.0102 at 0.44, 0.67, 0.87 and 1.02 μm, respectively. Such a level of accuracy is compatible with the accuracies of the AERONET retrievals based on sky radiances. The retrieval errors caused by instrument measurement errors appear to be insignificant for aerosol optical depths at 0.44 μm larger than 0.4.

The findings of this study have a practical application for studying aerosol radiative forcing both at the surface and at the TOA. It provides a more economical alternative to deriving both aerosol properties and aerosol radiative forcing over large areas. Aerosol optical depths measured by a hand-held sunphotometer (or placed on a solar tracker) can be combined with direct radiation measurements from a pyranometer to derive aerosol ω_o. For example, in the EAST-AIRE project, 25 hand-held sunphotometers have been deployed to obtain the spatial

distribution of aerosol loading across China (Xin et al. 2006). Some of the stations were equipped with pyranometers. Following this approach, we can derive ω_o across the region which is invaluable to address regional aerosol forcing issues.

Acknowledgments

The authors are grateful to X. Xia, P. Wang and H. Chen for operating the Xianghe site, B. Holben and T. Eck for the AERONET data, and M. Cribb for assistance in initial data processing. This study was conducted under the EAST-AIRE project sponsored by the NASA Radiation Science Program (NNG04GE79G) and the National Science Foundation of China (40250120071).

References

Ackerman, A. S., O. B. Toon, D. E. Stevens, A. J. Heymsfield, V.Ramanathan, and E. J. Welton (2000), Reduction of tropical cloudiness by soot, *Science*, *288*, 1042–1047.

Albrecht, B. A. (1989), Aerosols, cloud microphysics and fractional cloudiness, *Science*, *245*, 1227– 1230.

Bartsch, B., and J. Fischer (1997), Passive remote sensing of columnar water vapour content over land surfaces, *MPI Rep. 234*, 46 pp., Hamburg, Germany.

Bird, R. E., and R. L. Hulstrom (1982), Precipitable water measurements with sun photometers, *J. Appl. Meteor*., *21*, 1196–1201.

Boucher, O., and T. L. Anderson (1995), GCM assessment of the sensitivity of direct climate forcing by anthropogenic sulfate aerosols to aerosol size and chemistry, *J. Geophys. Res*., *100*, 26,117– 26,134.

Charlson, R. J., S. E. Schwartz, J. M. Hales, R. D. Cess, J. A. Coakley Jr., J. E. Hansen, and D. J. Hofmann (1992), Climate forcing by anthropogenic aerosols, *Science*, *255*, 423– 430.

Chylek, P., and J. A. Coakley, Jr. (1974), Aerosol and climate, *Science*, *183*, 75-77.

Coakley, J. A., Jr., R. D. Cess, and F. B. Yurevich (1983), The effect of tropospheric aerosol on the earth's radiation budget: A parameterization for climate models, *J. Atmos. Sci.*, *40*, 116–138.

Coakley, J. A., Jr., R. L. Bernstein, and P. A. Durkee (1987), Effects of ship-stack effluents on cloud reflectivity, *Science*, *237*, 1020– 1022.

Disney, M., P. Lewis, G. Thackrah, T. Quaife, and M. Barnsley (2004), Comparison of MODIS broadband albedo over an agricultural site with ground measurements and values derived from Earth observation data at a range of spatial scales, *Int. J. Remote Sensing*, *25***,** 5297-5317.

Dubovik, O., et al. (2000), Accuracy assessments of aerosol optical properties retrieved from Aerosol Robotic Network (AERONET) sun and sky radiance measurements, *J. Geophys. Res.*, *105*, 9791– 9806.

Dubovik, O., et al. (2002), Variability of absorption and optical properties of key aerosol types observed in worldwide locations, *J. Atmos. Sci*., *59*, 590– 608.

Eck, T. F., et al. (2005), Columnar aerosol optical properties at AERONET sites in central eastern Asia and aerosol transport to the tropical mid-Pacific, *J. Geophys. Res.*, *110*(D0), 6202, doi:10.1029/2004JD005274.

Gao, B.-C., and A. F. H. Goetz (1990), Column atmospheric water vapor and vegetation liquid water retrievals from airborne imaging spectrometer data, *J. Geophys. Res.*, *95*, 3549–3564.

Gao, B.-C., and J. Kaufman (1998), The MODIS near-IR water vapor algorithm, *Algorithm Technical Background Doc. ATBDMOD-03*, 25 pp.

Gao, B.-C., and J. Kaufman (2003), Water vapor retrievals using Moderate Resolution Imaging Spectroradiometer (MODIS) near infrared channels, *J. Geophys. Res.*, *108*, 4389, doi:10.1029/2002JD003023.

Halthore, R. N., T. F. Eck, B. N. Holben, and B. L. Markham (1997), Sun photometric measurements of atmospheric water vapor column abundances in the 940 nm band, *J. Geophys. Res.*, *102*, 4343–4352.

Haywood, J. M., P. N. Francis, M. D. Glew, and J. P. Taylor (2001), Optical properties and direct radiative effect of Saharan dust: A case study of two Saharan dust outbreaks using aircraft data, *J. Geophys. Res.*, *106*, 18 417–18 430.

Hansen, J., M. Sato and R. Ruedy (1997), Radiative forcing and climate response, *J. Geophys. Res*, *102*, 683 l-6864.

Holben, B., et al. (1998), A federated instrument network and data archive for aerosol characterization, *Remote Sens. Environ.*, *66*, 1– 16.

Intergovernmental Panel on Climate Change (IPCC) (2001), C*limate Change 2001, The Scientific Basis*, edited by J. T. Houghton et al., 881pp., Cambridge Univ. Press, New York, USA.

Jin, Y., B. Crystal, S, C. E. Woodcock, F. Gao, X. Li,and A H. Strahler (2003), Consistency of MODIS surface bidirectional reflectance distribution function and albedo retrievals:2. Validation, *J. Geophys. Res.*, *108*, D5,117– 26,134.

Kassianov, E. I., J. C. Barnard, and T. P. Ackerman (2005), Retrieval of aerosol microphysical properties using surface MultiFilter Rotating Shadowband Radiometer (MFRSR) data: Modeling and observations, *J. Geophys. Res.*, *110*, D09201, doi:10.1029/2004JD005337.

Kaufman, Y. J., D. Tanre, O. Dubovik, A. Karnieli, and L. A. Remer (2001), Absorption of sunlight by dust as inferred from satellite and groundbased remote sensing, *Geophys. Res. Lett.*, *28***,** 1479–1483.

Kaufman, Y. J., and B. C. Gao (1992), Remote sensing of water vapor in the near IR from EOS/MODIS, *IEEE Trans. Geosci. Remote Sens.*, *30*, 871–884.

Kaufman Y.J., G. P. Gobbi, I. Koren, 2005, Aerosol climatology using a tunable spectral variability cloud screening of AERONET data, *Geophy. Res. Lett.*, accepted. Dec 13 2005GL025478.

Kiehl, J. T., and B. P. Briegleb (1993), The relative roles of sulfate aerosols and greenhouse gases in climate forcing, *Science*, *260*, 311 – 314.

King, M. D., and B. M. Herman (1979), Determination of the ground albedo and the index of absorption of atmospheric particulates by remote sensing. Part I: Theory, *J. Atmos. Sci.*, *36*, 163-173.

King, M. D. (1979), Determination of the ground albedo and the index of absorption of atmospheric particulates by remote sensing. Part II: Application, *J. Atmos. Sci*., *36*, 1072-1083.

Kneizys, F. X., G.. P. Anderson, E. P. Shettle, W. O. Gallery, L. W. Abreu, J. E. A. Selby, J. H.Chetwynd and S. A. Clough (1988), Users Guide to Lowtran 7, *Environmental Research Papers, No.1010*, Air Force Geophysics Laboratory, Hanscom AFB, MA, USA.

Koepke, P., M. Hess, I. Schult, and E. P. Shettle (199), Global aerosol data set, *MPI Meteorologie Hamburg Rep. 243*, 44 pp.

Koepke, P., and M. Hess (1988), Scattering functions of tropospheric aerosols: The effects of nonsphererical particles, *Appl. Opt*., *27*, 2422-2430.

Li, Z. and L. Garand (1994), Estimation of surface albedo from space: A parameterization for global application, *J. Geophys. Res*., *99*, 8335–8350.

Li, Z., M. C. Cribb, and A.Trishchenko (2002), Influence of surface inhomogeneity on solar radiative transfer under overcast conditions. *J. Geophys. Res.*, *107*(D16), 4294, doi:10.1029/2001JD000976.

Li et al. 2006, Aerosol optical properties and radiative effects in Northern China, *J. Geophy. Res.*

Submitted to the same special issue.

Liang, S. (2003), A direct algorithm for estimating land surface broadband albedos from MODIS imagery, *IEEE Trans. Geosci. Remote Sensing*, *41*,136-145.

Liang, S., J. Stroeve and J. E. Box (2005), Mapping daily snow/ice shortwave broadband albedo from Moderate Resolution Imaging Spectroradiometer (MODIS): The improved direct retrieval algorithm and validation with Greenland in situ measurement, *J. Geophys. Res*., *110*, D10109, doi:10.1029/2004JD005493.

McClatchey, R.A., et al. (1972), Optical properties of the atmosphere, *Environ. Res. Pap. 411*,108 pp., Air Force Cambridge Res. Lab., Bedford, Mass., USA.

Menon, S., J. Hansen, L. Nazarenko, and Y. Luo (2002), Climate effects of black carbon aerosols in China and India, *Science*, *297*, 2250-2253.

Michalsky, J. J., J. C. Liljegren, and L. C. Harrison (1995), A comparison of sun photometer derivations of total column water vapor and ozone to standard measures of same at the Southern Great Plains Atmospheric Radiation Measurement site. *J. Geophys. Res.*, *100***,** 25, 995–26,003.

Mishchenko, M. I., A.A. Lacis, B.E. Carlson, and L. D. Travis (1995), Nonsphericity of dust-like tropospheric aerosols: Implications for aerosol remote sensing and climate modeling, *Geophys. Res. Lett*., *22*, 1077-1080.

Mishchenko, M., L. D. Travis, R. A. Kahn, and R. A. West (1997), Modeling phase functions for dustlike tropospheric aerosols using a shape mixture of randomly oriented polydispersed spheroids, *J. Geophys. Res*., *102*, 16,831– 16,847.

Morys, M., F. M. Mims III, S. Hagerup, S. E. Anderson, A. Baker, J. Kia, and T. Walkup (2001), Design, calibration, and performance of Microtops II handheld ozone monitor and sun photometer, *J. Geophys. Res.*, *106*, 14 573–14 582.

Nakajima, T.and M. Tanaka (1988), Algorithms for radiative intensity calculations in moderately thick atmospheres using a truncation approximation, *J. Quant. Spectrosc. Radia*t. *Transfer, 40*, 51-69.

Patterson, E. M., and D. A. Gillette, and B. H. Stockton (1977), Complex index of refraction between 300 and 700 for Saharan aerosols, *J. Geophys. Res*., *82*, 3153–3160.

Schwartz, S. E. (1996), The Whitehouse effect—Short-wave radiative forcing of climate by

anthropogenic aerosols: An overview, *J. Aerosol Sci.*, *27*, 359– 382.

Shettle, E. P., and R. W. Fenn (1979), Models of aerosols of lower troposphere and the effect of humidity variations on their optical properties, *AFCRL Tech. Rep. 79 0214*, 100 pp., Air Force Cambridge Research Laboratory, Hanscom Air Force Base, Mass., USA.

Silva, A. M., M. L. Bugalho, M. J. Costa, W. von Hoyningen-Huene, T. Schmidt, J. Heintzenberg, and S. Henning (2002), Aerosol optical properties from columnar data during the second Aerosol Characterization Experiment on the south coast of Portugal, *J. Geophys. Res.*, *107*, D224642, doi:10.1029/2002JD002196.

Tanre, D., and Coauthors (2001), Climatology of dust aerosol size distribution and optical properties derived from remotely sensed data in the solar spectrum. *J. Geophys. Res.*, *106*, 18,205–18,217.

Twomey, S. A. (1977), The influence of pollution on the shortwave albedo of clouds, J. Atmos. Sci., *34*, 1149– 1152.

Twomey, S. A., M. Piepgrass, and T. L. Wolfe (1984), An assessment of the impact of pollution on the global albedo, *Tellus, Ser. B*, *36*, 356–366.

Volz, F.E. (1974), Economical multispectral sunphotometer for measurements of aerosol extinction from 0.44 mm to 1.6 mm and precipitable water, *Appl. Opt*., *13*, 1732–1733.

World Meteorological Organization (1983), Radiation commission of IAMAP meeting of experts on aerosol and their climatic effects, *World Meteorological Organization Rep. WCP55*, 28–30.

Xin, et al. (2006), The optical depth and Angstrom exponent of aerosols observed in a network of hand-held sun photometers in China, *J. Geophy. Res*, special issue on EAST-AIRE, revised.

Zhao, F., and T. Nakajima (1997), Simultaneous determination of water leaving reflectance and aerosol optical thickness from CZCS measurements, *Appl.Opt*., *36*, 6949-6956.

Zhao F., Y. Li, C. Dong (2002), An algorithm for the determination of aerosol optical thickness from AVHRR imagery over oceans, *Meteorology and Atmospheric Physics*, *80*, 73-88.

Table 1. Retrieval error $\delta\omega_o$ arising from CM21 measurement errors.*

τ(0.5μm)	0.1	0.4	0.8	1.2
$\delta\omega_o$(0.5μ m)	0.103	0.028	0.016	0.012

* In the calculation of the retrieval error $\delta\omega_o$, the CM21 measurement error is set at 8 Wm^{-2}. The solar zenith angle is 50^o and the Angstrom exponent is 1.2. The 'true' aerosol single scattering albedo is 0.919.

Figure Captions

Figure 1. Broadband downwelling shortwave flux at λ=0.5μm as a function of aerosol optical depth for (a) different values of the aerosol single scattering albedo, (b) different values of the imaginary part of the index of refraction, (c) different aerosol size distributions and (d) different values of the surface albedo.

Figure 2. Statistics associated with the retrieved aerosol single scattering albedo at 0.5μm.

Figure 3. Scatterplots between (a) aerosol single scattering albedo at λ=0.5μm and Angstrom exponent, (b) aerosol single scattering albedo and aerosol optical depth and (c) Angstrom exponent and aerosol optical depth.

Figure 4. (a) Daily-averaged single scattering albedo at Xianghe, China for the period of September 2004 to August 2005 and (b) seasonally-averaged aerosol single scattering albedo for the same data as in Figure 4a.

Figure 5. Comparison between the aerosol single scattering albedo retrieved from the proposed algorithm and AERONET products at wavelengths of (a) 0.44 μm, (b) 0.67 μm, (c) 0.87 μm and (d) 1.02 μm. To match the times for comparison purposes, the values of the single scattering albedo retrieved by the proposed algorithm were averaged over a period of 30 minutes before

and after the times corresponding to the AERONET retrievals.

Figure 6. Comparison between the aerosol single scattering albedo retrieved using the proposed algorithm and AERONET products at wavelengths (a) 0.44 μm, (b) 0.67 μm, (c) 0.87 μm and (d) 1.02 μm. In this figure, broadband downwelling shortwave fluxes were simulated using aerosol size distributions and values of the aerosol index of refraction retrieved at the Xianghe site by AERONET. The simulated broadband fluxes were then employed in conjunction with the AERONET aerosol optical depth and Angstrom exponent products, to retrieve the single scattering albedo using the proposed algorithm.

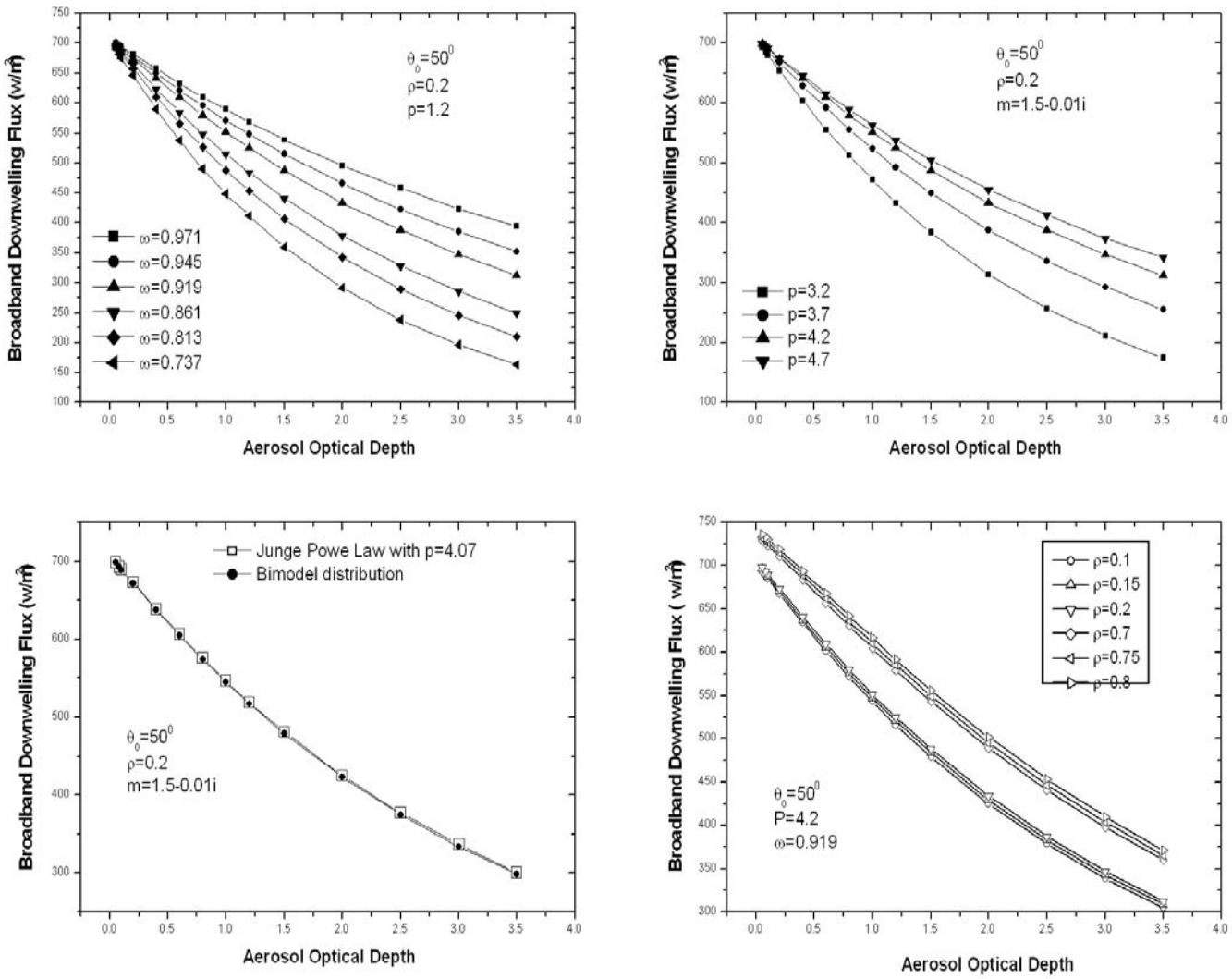

Figure 1. Broadband downwelling shortwave flux as a function of aerosol optical depth for (a) different values of the aerosol single scattering albedo, (b) different values of the imaginary part of the index of refraction, (c) different aerosol size distributions and (d) different values of the surface albedo.

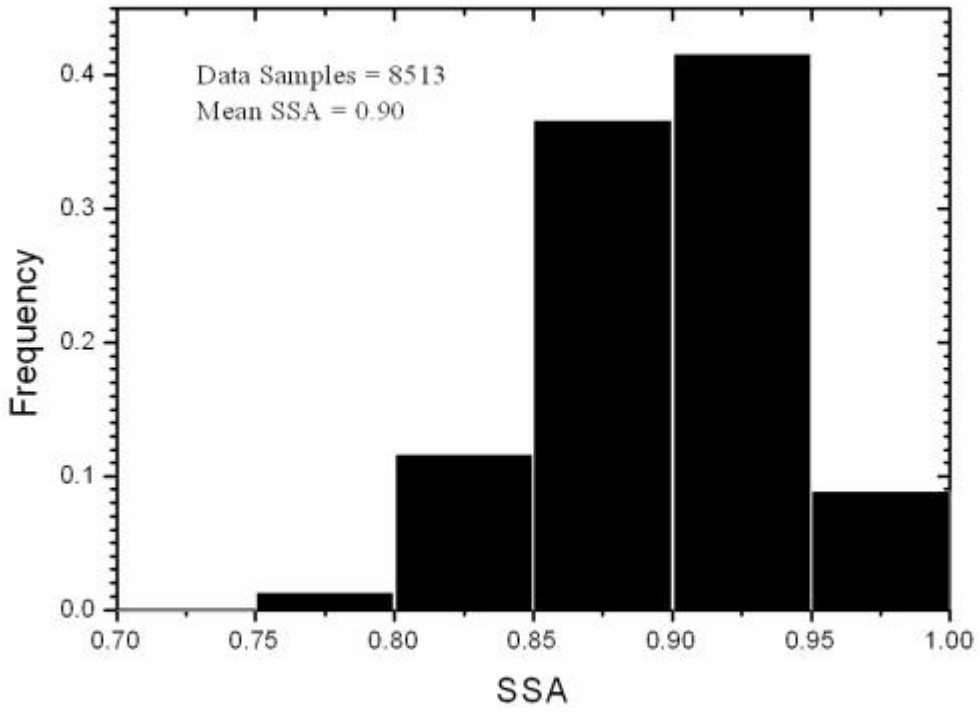

Figure 2. Statistics associated with the retrieved aerosol single scattering albedo.

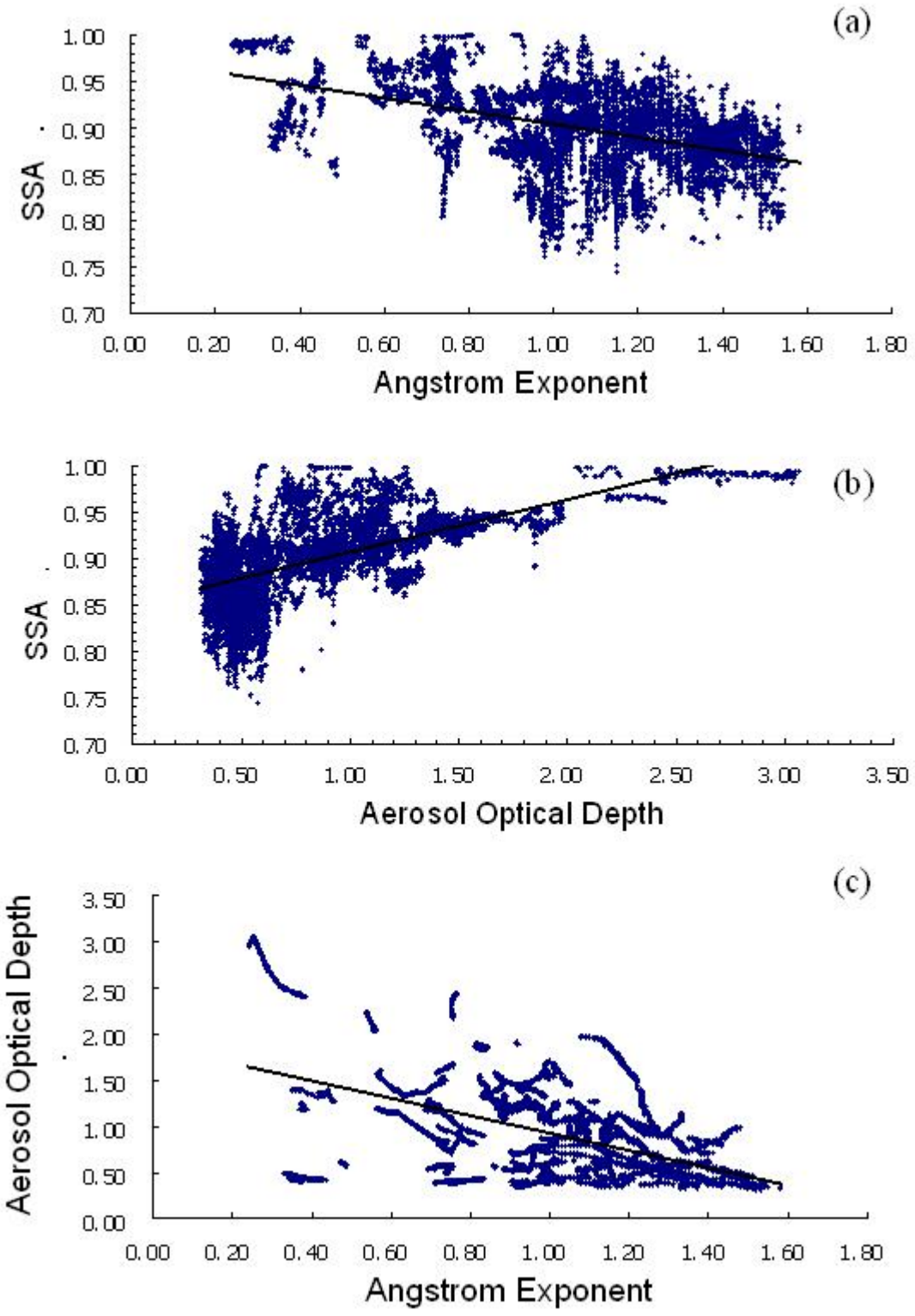

Figure 3. Scatterplots between (a) aerosol single scattering albedo and Angstrom exponent, (b) aerosol single scattering albedo and aerosol optical depth and (c) Angstrom exponent and aerosol optical depth.

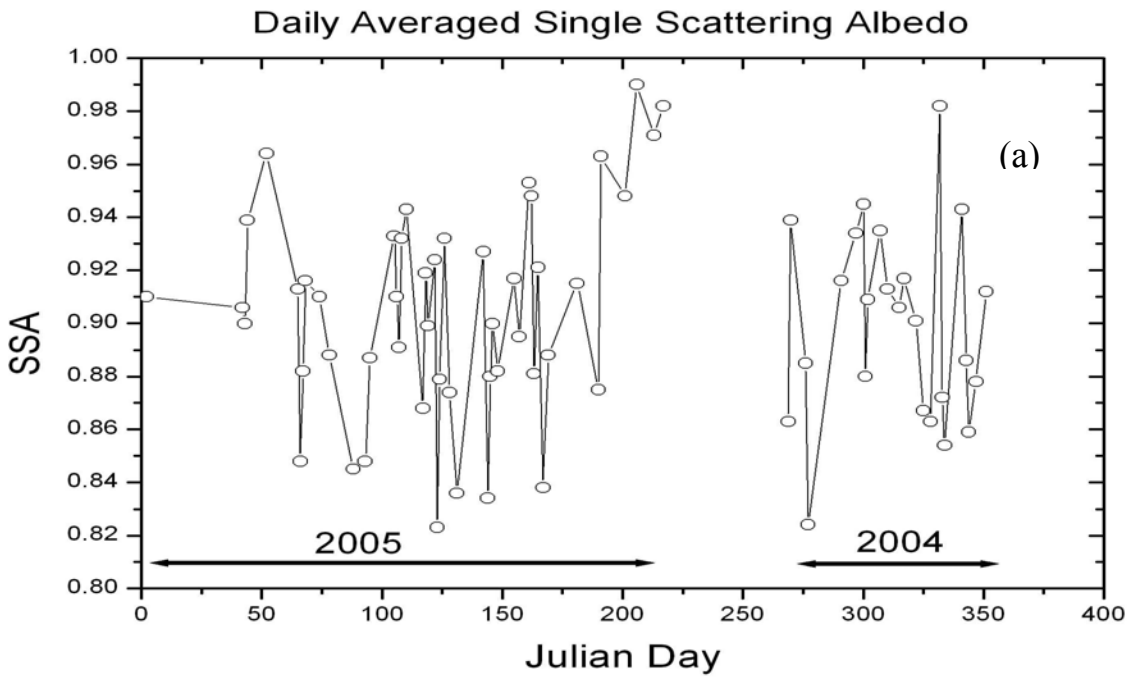

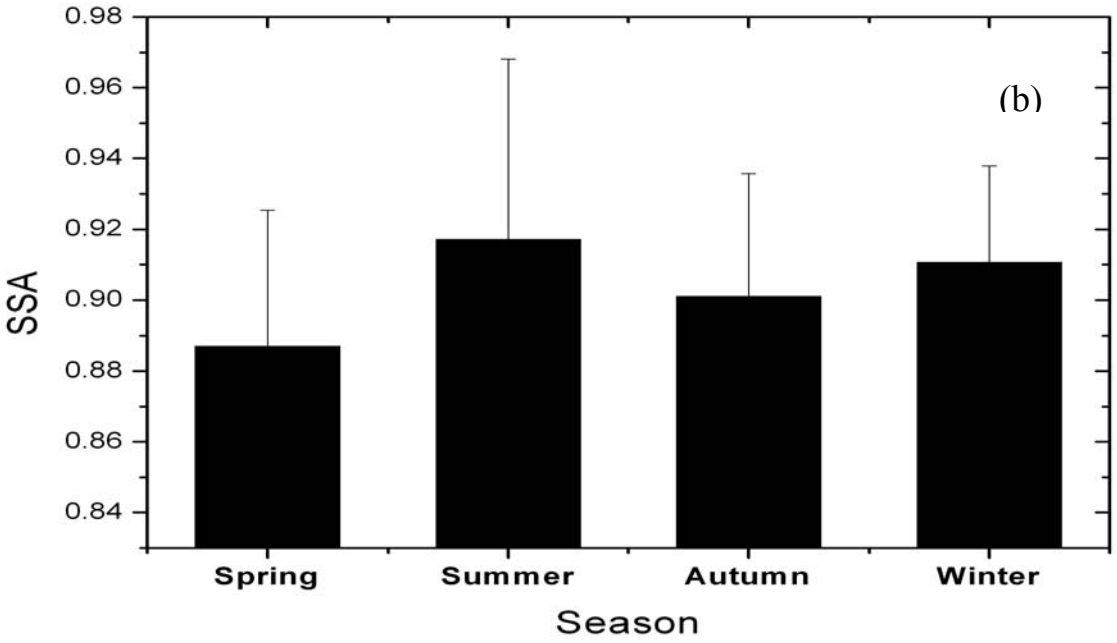

Figure 4. (a) Daily-averaged single scattering albedo at Xianghe, China for the period of September 2004 to August 2005 and (b) seasonally-averaged aerosol single scattering albedo for the same data as in Figure 4a.

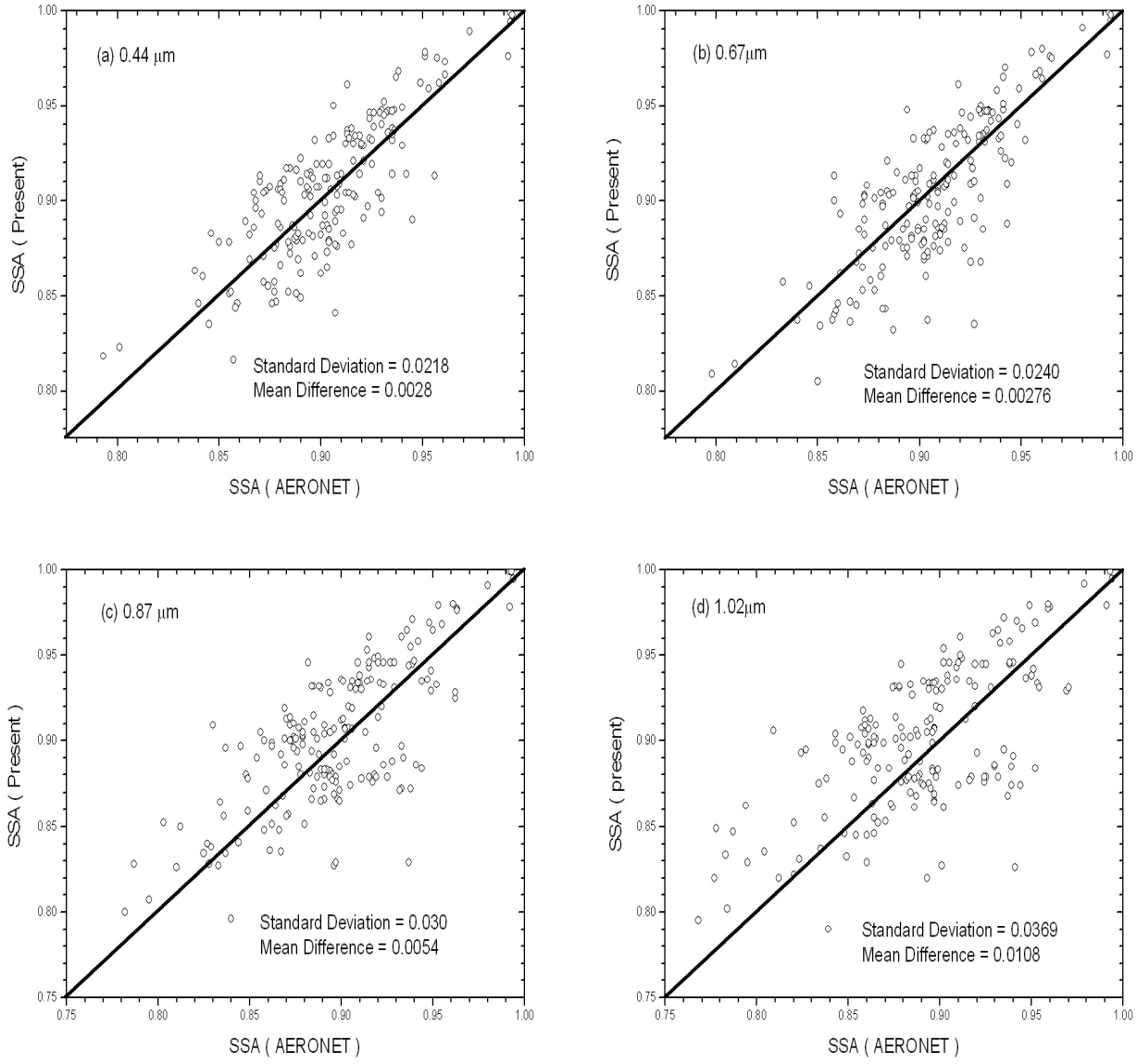

Figure 5. Comparison between the aerosol single scattering albedo retrieved from the proposed algorithm and AERONET products at wavelengths of (a) 0.44 μm, (b) 0.67 μm, (c) 0.87 μm and (d) 1.02 μm. To match the times for comparison purposes, the values of the single scattering albedo retrieved by the proposed algorithm were averaged over a period of 30 minutes before and after the times corresponding to the AERONET retrievals.

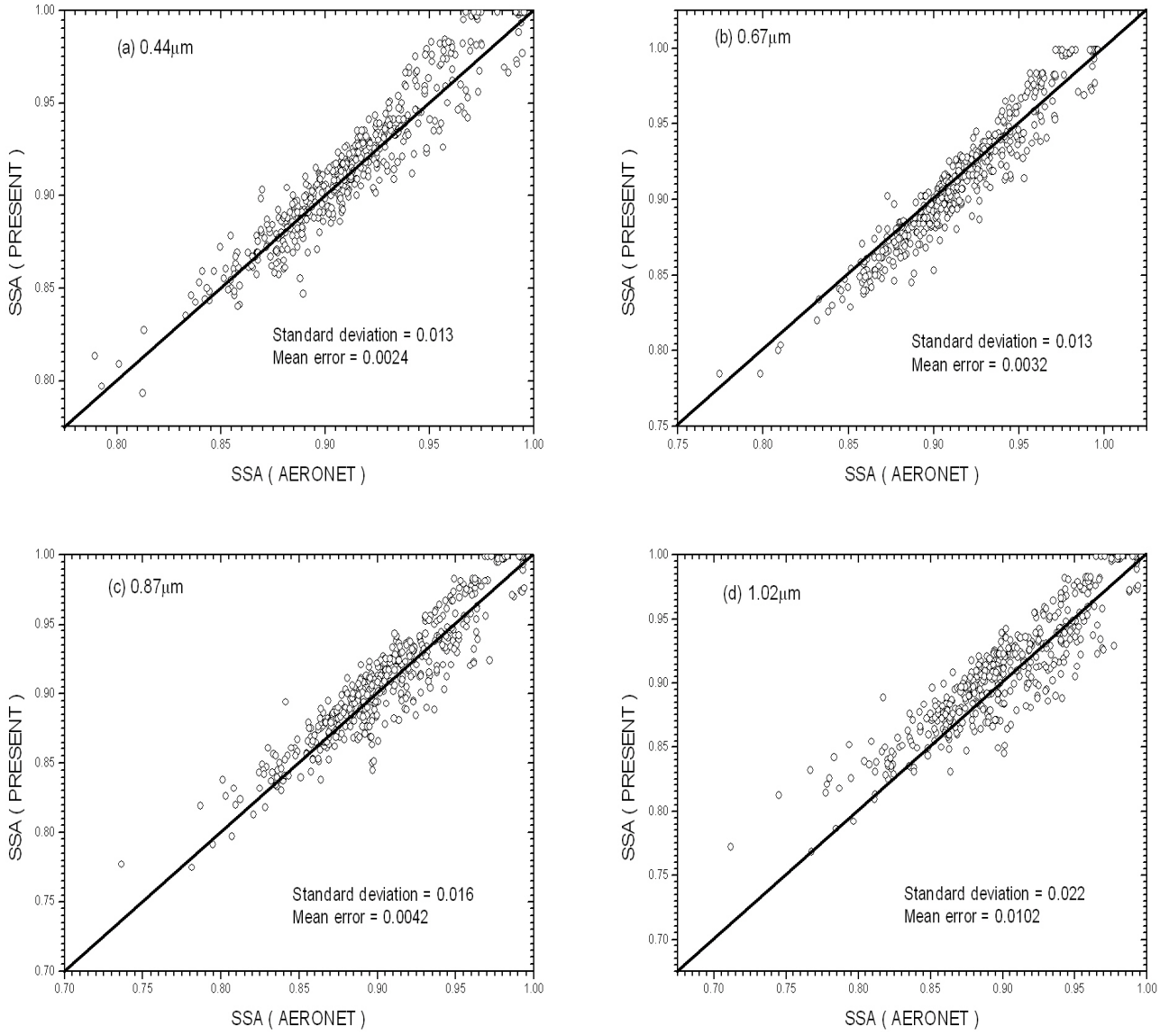

Figure 6. Comparison between the aerosol single scattering albedo retrieved using the proposed algorithm and AERONET products at wavelengths (a) 0.44 μm, (b) 0.67 μm, (c) 0.87 μm and (d) 1.02 μm. In this figure, broadband downwelling shortwave fluxes were simulated using aerosol size distributions and values of the aerosol index of refraction retrieved at the Xianghe site by AERONET. The simulated broadband fluxes were then employed in conjunction with the AERONET aerosol optical depth and Angstrom exponent products, to retrieve the single scattering albedo using the proposed algorithm.

1